CHEMISTRY
A EUROPEAN JOURNAL

DOI: 10.1002/chem.200600699

# Exploring Base-Pair-Specific Optical Properties of the DNA Stain Thiazole Orange

**Dilip Venkatrao Jarikote,[a] Nils Krebs,[b] Sebastian Tannert,[b] Beate Röder,[b] and Oliver Seitz*[a]**

**Abstract:** Double-stranded DNA offers multiple binding sites to DNA stains. Measurements of noncovalently bound dye–nucleic acid complexes are, necessarily, measurements of an ensemble of chromophores. Thus, it is difficult to assign fluorescence properties to base-pair-specific binding modes of cyanine dyes or, vice versa, to obtain information about the local environment of cyanines in nucleic acids by using optical spectroscopy. The feasibility to stain DNA and simultaneously probe local perturbations by optical spectroscopy would be a valuable asset to nucleic acid research. So-called FIT probes (forced intercalation probes) were used to pinpoint the location of the DNA stain thiazole orange (TO) in PNA·DNA duplexes. A detailed analysis of the base-pair dependence of optical properties is provided and enforced binding of TO is compared with "classical" binding of free TO-PRO1. UV-visible absorbance, circular dichroism (CD) and fluorescence spectroscopy, and melting-curve analyses confirmed site-specific TO intercalation. Thiazole orange exhibited base-specific responses that are not observed in noncovalent dye–nucleic acid complexes, such as an extraordinary dependence of the TO extinction coefficient (±60% variation of the averaged $\varepsilon_{max}$ of 57000 $M^{-1}cm^{-1}$) on nearest-neighbor base pairs. TO signals hybridization, as shown by increases in the steady-state fluorescence emission. Studies of TO fluorescence lifetimes in FIT–PNA and in DNA·DNA and PNA·DNA complexes highlighted four different fluorescence-decay processes that may be closed or opened in response to matched or single-mismatched hybridization. A very fast decay process (0.04–0.07 ns) and a slow decay process (2.33–3.95 ns) provide reliable monitors of hybridization, and the opening of a fast decay channel (0.22–0.48 ns) that resulted in an attenuation of the fluorescence emission is observed upon the formation of mismatched base pairs.

**Keywords:** cyanines · DNA · dyes/pigments · fluorescence · nucleic acids

## Introduction

The advancements in bioscience would not have been possible without simple methods for detecting and visualizing biomolecules, such as DNA and RNA. Staining of nucleic acids is usually achieved by the use of fluorescent or strongly absorbing chromophores.[1] Asymmetric cyanine dyes, such as oxazole yellow (YO and its dimer YOYO), thiazole orange (TO and its dimer TOTO), SYBR Green or PicoGreen are particularly interesting because of their extraordinary increase in fluorescence upon binding to nucleic acids.[2–6] This property has led to advancements in countless applications in molecular biology, such as DNA quantification in the homogenous phase and in gels, real-time polymerase chain reaction, and in DNA-binding and DNA-damage assays. Binding of cyanine dyes to nucleic acids has been widely investigated, and oxazole yellow and thiazole orange are probably amongst the most studied asymmetric cyanines.[7–15] The monomeric cyanines bind DNA in different ways; intercalation between base pairs, association to the minor groove as monomers, dimers, and higher aggregates, and probably also by interaction of positively charged dyes with the negatively charged ribosephosphate backbone.[7,9,10,46] A great deal of research has been devoted to the base-pair specificity of DNA binding. Although preferred binding motifs have been found for dimeric bisintercalators, such as YOYO and TOTO,[16–20] there is no conclusive evidence yet for sequence-specific binding of the monomeric forms YO and TO. Measurements of noncovalently bound

[a] D. V. Jarikote, Prof. Dr. O. Seitz
Institut für Chemie, Humboldt-Universität zu Berlin
Brook-Taylor-Str. 2, 12489 Berlin (Germany)
Fax: (+49) 30-2093-7266
E-mail: oliver.seitz@chemie.hu-berlin.de

[b] N. Krebs, S. Tannert, Prof. Dr. B. Röder
Institut für Physik, Humboldt-Universität zu Berlin
Newtonstr. 15, 12489 Berlin (Germany)

dye–nucleic acid complexes are measurements of an ensemble of chromophores located at various binding sites. Thus, it has not been possible to assign optical properties, such as the observed fluorescence, to base-specific binding modes of YO and TO or, vice versa, to obtain information about the local environment of cyanines in nucleic acids by using optical spectroscopy.

Sequence-specific binding can be achieved by linking cyanine dyes to oligonucleotides or analogues thereof.[21–33] Usually, cyanine dyes or other DNA stains[34,35] have been linked to nucleic acids by means of a flexible tether. Previous work by ourselves and others has shown that the tether plays an important role as far as the responsiveness of fluorescence and the stability of probe–target duplexes are concerned.[28,36,37] Long tethers provide sufficient flexibility to allow multiple binding modes. We have developed probes, so-called FIT probes (forced intercalation probes), in which, contrary to alternative cyanine–nucleic acid conjugates, the flexibility is constrained by linking thiazole orange as a surrogate fluorescent base.[22,38] Previous studies demonstrated the synthesis[39] and useful features, such as high affinity of FIT–PNA to complementary DNA, nondiscriminate pairing of TO to all canonical DNA bases,[38] high specificity for complementary sequences, and enhancement of steady-state fluorescence emission upon formation of matched probe–target complexes with attenuated fluorescence in response to binding to single-nucleobase-mismatched targets.[37,40] One of the intriguing opportunities provided by such base replacement is to localize cyanine dyes to a specific site in the nucleic acid duplex and to assess the optical properties of this isolated binding mode without the problem of competition from other binding sites. Here we provide a detailed analysis of the base-pair dependence of the UV-visible absorbance, steady-state and time-resolved fluorescence-emission properties and compare enforced binding of thiazole orange with the "classical mode" binding of free TO-PRO1. Forced intercalation demonstrates, for the first time, the influence of specific base pairs on the decay processes of the TO excited state. Furthermore, interactions between TO and nucleobases can result in closing and, perhaps surprisingly, opening of decay channels, and the balance between these processes determines the fluorescence output. We also explored the decay processes that are most responsive to local perturbations introduced by the presence of mismatched base pairs.

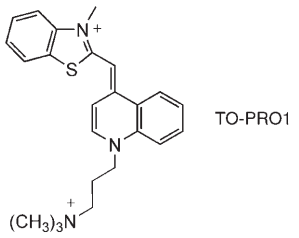


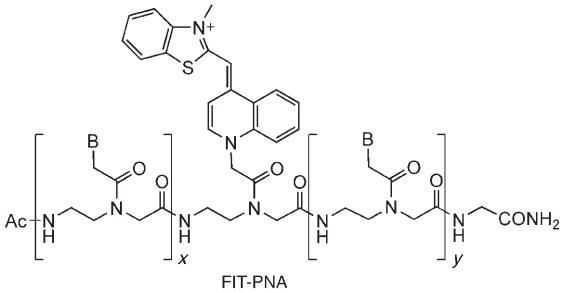


FIT-PNA

## Results

In duplexes containing TO–PNA conjugates, such as FIT–PNA thiazole orange can be embedded specifically between two selected base pairs. Thus, it is possible to explore the responsiveness of the optical properties of thiazole orange to defined changes in the local environment. In FIT–PNA·DNA duplexes shown in Figure 1 one strand is comprised of the nucleic acid analogue PNA. This is in contrast to the binding of the DNA stain TO–PRO1 to nucleic acid double strands, which results in the formation of an ensemble of different dye–nucleic acid adducts. To account for the changes introduced by the introduction of the noncharged PNA backbone, the unconstrained binding of TO–PRO1 to both DNA·DNA (**1·2**) and PNA·DNA (**3·2**) duplexes was studied. Thiazole orange (TO) in FIT–PNA **4** was placed opposite to thymine. A previous study suggested that the influence of the pairing partner on the optical properties of TO is small relative to the influence of intrastrand stacking partners.[40]

**Absorbance**: Previous spectroscopic studies of monomeric thiazole orange TO and TO–PRO1 provided insight into the characteristics of thiazole orange binding to duplex DNA.[9–11] Figure 2A shows the absorption spectrum of 0.5 μM free TO–PRO1 in aqueous buffer. The dye exists as monomer under these condition, as indicated by the broad band in the visible region with one peak at 508 nm and a small shoulder at $\lambda \approx 485$ nm. As duplex DNA **1·2** was added, the absorption band underwent a gradual bathochromic shift. As the concentration of duplex increased, the shoulder at 490 nm became more pronounced. Under saturation conditions the addition of DNA·DNA duplex **1·2** resulted in a 10-nm bathochromic shift and a decrease in absorbance at 508 nm of 27% (Table 1). This data is in agreement with previous spectroscopic studies of TO–PRO1/DNA binding.[9] A similar reduction (34%) in absorbance at 508 nm was observed upon addition of PNA·DNA duplex **3·2** (Figure 2B). However, the bathochromic shift was smaller (4 nm), the blue side-shoulder at 490 nm was less pronounced, and no increase in absorbance at 520 nm was observed.

Interestingly, the absorbance of TO in single-stranded PNA conjugates **4**tt, **4**at, **4**cc, and **4**aa was significantly lower than the absorbance of TO–PRO1 in the presence of duplex nucleic acids, and the shoulder at $\lambda \approx 485$ nm became more

  

**1**, DNA 5'–G–C–C–G–T–A–A–T–A–G–C–C–G–3'
**2**, DNA '3–C–G–G–C–A–T–T–A–T–C–G–G–C–5'

**3**, PNA Ac–g–c–c–g–t–a–a–t–a–g–c–c–g–$Gly^{CONH_2}$
**2**, DNA '3–C–G–G–C–A–T–T–A–T–C–G–G–C–5'

**4**, FIT-PNA Ac–g–c–c–g–t–*k*–**TO**–*l*–t–a–g–c–c–g–$Gly^{CONH_2}$
**2**, DNA '3–C–G–G–C–A–*M*–T–*N*–A–T–C–G–G–C–5'

| matched duplex | | mismatched duplex | |
|---|---|---|---|
| **4**aa | —a·**TO**-a— | **4**aa | —a·**TO**-a— |
| **2**TT | —T–T–T— | **2**TC | —T–T–C— |
| **4**tt | —t-**TO**-t— | **4**tt | —t-**TO**-t— |
| **2**AA | —A–T–A— | **2**AC | —A–T–C— |
| **4**gg | —g·**TO**-g— | **4**gg | —g·**TO**-g— |
| **2**CC | —C–T–C— | **2**CG | —C–T–G— |
| **4**cc | —c·**TO**-c— | **4**cc | —c·**TO**-c— |
| **2**GG | —G–T–G— | **2**GC | —G–T–C— |
| **4**at | —a·**TO**-t— | **4**at | —a·**TO**-t— |
| **2**TA | —T–T–A— | **2**TC | —T–T–C— |
| **4**ag | —a·**TO**-g— | **4**ag | —a·**TO**-g— |
| **2**TC | —T–T–C— | **2**TG | —T–T–G— |
| **4**ac | —a·**TO**-c— | **4**ac | —a·**TO**-c— |
| **2**TG | —T–T–G— | **2**TC | —T–T–C— |
| **4**gc | —g·**TO**-c— | **4**gc | —g·**TO**-c— |
| **2**CG | —C–T–G— | **2**CC | —C–T–C— |

**5**, FIT-PNA Ac–g–c–c–g–t–a–**TO**–*l*–a–g–c–c–g–$Gly^{CONH_2}$
**6**, DNA '3–C–G–G–C–A–T–*N*–A–T–C–G–G–C–5'

| matched duplex | | abasic duplex | |
|---|---|---|---|
| **5**t | —**TO**-t— | **5**t | —**TO**-t— |
| **6**TA | —T–A— | **6**HA | —H–A— |
| **5**h | —**TO**-h— | | |
| **6**TA | —T–A— | | |

h = 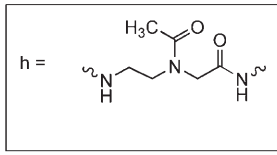

H = 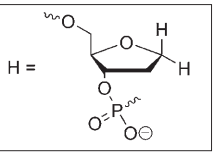

Figure 1. Nucleic acids and nucleic acid–dye conjugates studied. (a, c, g, and t specify PNA monomers; *k* and *l* indicate wildcard sites in PNA; A, C, G, and T specify nucleotides in DNA; *M* and *N* indicate wildcard sites in DNA; TO is the thiazole orange PNA monomer.

pronounced (Figure 3). The absorption maximum of TO–PNA conjugates **4** and their DNA complexes **4**·**2** are red-shifted by 6–11 nm relative to the UV spectra of free TO–PRO1 (Table 2). Most remarkable was the observation that TO absorbance in FIT–PNA varied strongly as the nearest-neighbor bases were changed. For example, TO absorbance was lowest in PNA **4**tt, which featured TO flanked by two thymine residues. Twice as much TO absorbance was observed in PNA **4**cc and **4**aa containing TO embedded between two cytosine or adenine bases, respectively. Very strong absorbance (three-fold higher than for **4**tt) was measured for **4**gc, **4**gg, and **4**ag, in which TO was next to one or two guanine bases. The pronounced nearest-neighbor dependence of TO absorbance in FIT–PNA complexes **4** may indicate electronic coupling with the nucleobases.

The addition of complementary DNA **2** to the FIT–PNA single strands **4** resulted in significant increases in TO absorbance at 515 nm of 18–53 % (Figure 4A–H). A blue-shift of 3 and 2 nm was observed upon hybridization of FIT–PNA **4**at, **4**ac, and **4**aa featuring an a-TO-t, a-TO-c, and a-TO-a motif, respectively. Overall, the band shapes of TO absorption in FIT–PNA·DNA duplexes **4**·**2** resembled more closely that of TO–PRO1 bound to DNA·DNA than that of TO–PRO1 bound to PNA·DNA. TO has been reported to exhibit environmentally sensitive absorption spectra. For example, $\varepsilon_{max}$ of TO noncovalently bound to poly(dG–dC) duplexes was 16 % higher than that of TO bound to poly(dA–dT) duplexes.[10] A markedly more pronounced trend was observed in single-stranded FIT–PNA, in which $\varepsilon_{max}$ of g-TO-c exceeded that of a-TO-t by 200 % (Table 2). This remarkably high responsiveness of TO absorbance may indicate tighter stacking interactions between TO and nucleobases in both single-stranded and DNA-complexed FIT–PNA than of TO noncovalently associated with DNA·DNA and PNA·DNA duplexes.

**Circular dichroism (CD) spectroscopy**: CD spectra were measured to obtain insight into possible modes of TO–nucleic acid interactions. Figures 5A and B show the induced CD spectra of TO–PRO1 due to binding to DNA·DNA and PNA·DNA duplexes, respectively, at low dye/base-pair ratios. At high dye/base-pair ratios two bands of different sign appear. Such a structure can originate from a superimposed exciton CD induced by dye–dye interactions in the minor groove.[7] In the PNA·DNA duplex the CD couplet is observed at lower dye/base-pair ratios (d/bp = 1:4) than in the DNA·DNA duplex (1:2.5). This observation suggests that, for the sequence studied, association of TO–PRO1 in the PNA·DNA minor groove may occur at lower dye concentration than in the DNA·DNA minor groove. The TO chromophore in the FIT–PNA·DNA complex **5**t·**6**TA shows a negative band with a maximum at 514 nm, and in the FIT–PNA·DNA complex **4**gc·**2**CG, the band is at 518 nm, which coincide with the absorption bands (Figure 5C). Negative bands have been assigned to the intercalation mode.[7,11,13] We concluded that the TO chromophore in **5**t·**6**TA and **4**gc·**2**CG predominantly accommodates an intercalated position in the interior of the duplex. In contrast, the mode of binding of TO–PRO1 to DNA·DNA and PNA·DNA appears less-clearly defined.

**$T_M$ measurements**: Further support for the intercalation of TO in FIT–PNA·DNA duplexes came from thermal-stability measurements. Previous work has shown that the introduction of TO as a surrogate base does not affect the stability of PNA·DNA duplexes and that each of the four canonical nucleobases A, C, G, and T was tolerated well if positioned opposite to TO.[38] Melting-curve experiments with duplexes **5**t·**6**TA, **5**t·**6**HA, and **5**h·**6**TA were performed to evaluate the influence of TO-base-pairing and TO-base-stacking

  

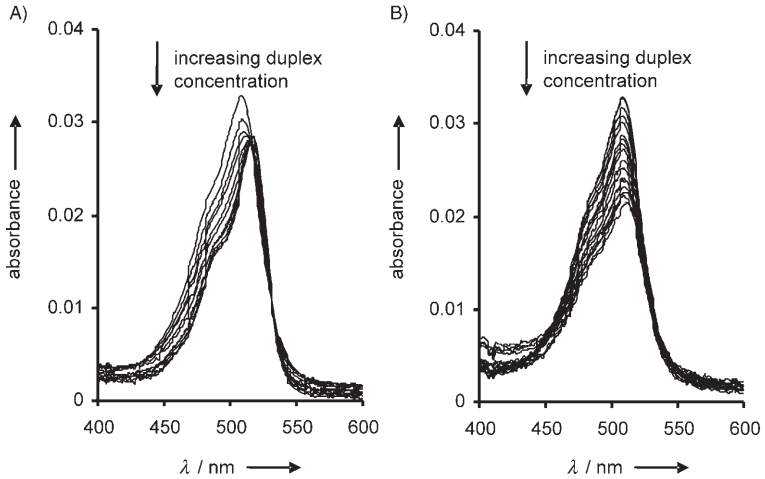


Figure 2. Absorbance of TO–PRO1 before and after addition of: A) DNA·DNA duplex **1·2** (0.1, 0.2, 0.3, 0.5, 0.7, 1.0, 1.5, 2.0, 2.5, 3.0, and 4.0 μM) and B) PNA·DNA duplex **3·2** (0.1, 0.2, 0.3, 0.5, 0.7, 1.0, 1.5, 2.0, 2.5, 3.0, 4.0, 5.0, 6.0, 8.0, 10.0, 12.0, and 14.0 μM). Measurement conditions: 0.5 μM TO–PRO1 in degassed buffer (NaCl (100 mM), $NaH_2PO_4$ (10 mM) at pH 7.0).

Table 1. Spectroscopic parameters of TO–PRO1 before and after addition of DNA·DNA (**1·2**) and PNA·DNA (**3·2**) duplexes.

| Substrate | $\lambda_{max(abs)}$ [nm][a] | $\varepsilon_{508}$ [$M^{-1}cm^{-1}$][b] | $\lambda_{max(em)}$ [nm][c] | $\phi_{em}$[d] | $K_{app}$ [μM per bp][e] |
|---|---|---|---|---|---|
| TO–PRO1 | 508 | 63000 | 530 | $1.4\times10^{-4}$[f] | – |
| TO–PRO1 + **1·2** | 518 | 46000 | 530 | 0.21 | 134 ± 20 |
| TO–PRO1 + **3·2** | 512 | 42000 | 534 | 0.02 | 7.3 ± 0.4 |

[a] Wavelength of absorbance maximum. [b] Extinction coefficient at 508 nm. [c] Wavelength of fluorescence-emission maximum. [d] Fluorescence quantum yield. [e] Apparent affinity constant obtained from Scatchard analysis. [f] From ref. [9].

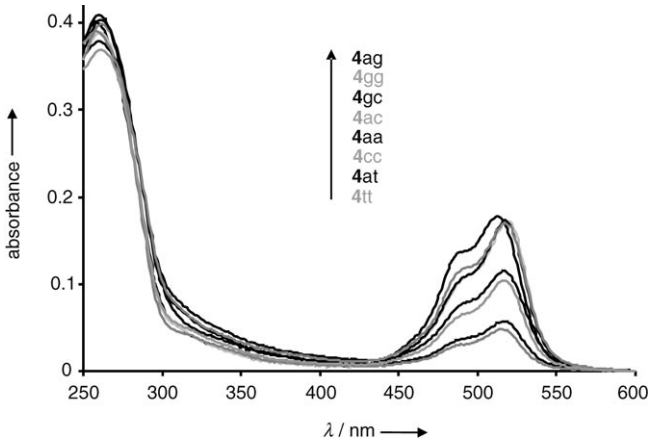


Figure 3. Absorbance spectra of single-stranded PNA–TO conjugates **4**. Absorbance at 600 nm was set to zero and absorbance curves were calibrated to the calculated $\varepsilon_{260}$. Measurement conditions: 3 μM FIT–PNA in degassed buffer (NaCl (100 mM), $NaH_2PO_4$ (10 mM) at pH 7.0).

(Table 3). Comparison of the $T_M$ measured for duplex **5t·6**HA that was devoid of a "TO pairing partner" (71 °C) with the $T_M$ determined for duplex **5t·6**TA, in which TO was opposite to thymine (68 °C), suggests that intercalation of the TO chromophore is even more facile if the steric demand exerted by an opposing base is reduced. The removal of a nucleobase adjacent to intercalated TO should lower the duplex stability due to a lack of stacking interactions. Indeed, the $T_M$ of duplex **5h·6**TA, in which one of the intrastrand stacking partners of TO has been removed, is 9 °C lower than the $T_M$ of the FIT–PNA·DNA duplex **5t·6**TA.

**Fluorescence spectroscopy**: The particular features of TO as a surrogate base were explored further by comparing the fluorescence spectra of TO in response to "unconstrained" and "enforced" (FIT–PNA) binding. The fluorescence quantum yield of free TO–PRO1 was determined previously to be extremely low ($\phi_{em}=1.4\times10^{-4}$).[9] As expected, addition of duplex DNA **1·2** to free dye led to dramatic increases in fluorescence intensity (Figure 6A) and fluorescence quantum yield ($\phi_{em}=$ 0.21, Table 1). Interestingly, the fluorescence of TO–PRO1 also increased ($\phi_{em}=0.02$) if TO–PRO1 was allowed to bind to PNA·DNA duplex **3·2** (Figure 6B, Table 1). This is noteworthy in light of previous investigations in which typical intercalators, such as ethidium bromide, 8-methoxypsoralen, and $Ru(phen)_2dppz^{2+}$, did not exhibit increases in fluorescence upon exposure to PNA·DNA duplexes.[41] However, analysis of the fluorescence titration data (Figure 6C, D) revealed that TO–PRO1 binds PNA·DNA duplex **3·2** with lower affinity ($K_{app}=7.3\pm$ 0.4 μM per base pair) than DNA·DNA duplex **1·2** ($K_{app}=$ 134 ± 20 μM per base pair) (Table 1). Most remarkable were the results obtained with FIT–PNA complexes **4**. The TO dye in conjugates **4** had a higher fluorescence quantum yield ($\phi_{em}=0.03$–0.05) than free TO–PRO1, which indicates TO-base-stacking in the single-stranded form (Table 2). However, the formation of FIT–PNA·DNA duplexes **4·2** was accompanied by significant increases in fluorescence intensity owing to the high fluorescence quantum yields ($\phi_{em}=0.12$–0.27) in the double-stranded form. Measurements of PNA–TO conjugates **4** in which the TO stacking partner was varied revealed the nearest-neighbor dependence of the TO fluorescence quantum yields (Table 2). The lowest fluorescence quantum yield ($\phi_{em}=0.13$) within the sequences studied was obtained if TO was embedded between two cytosines. The intercalation between two guanines or two thymines resulted in higher $\phi_{em}$; 0.16 and 0.20, respectively.

  

Table 2. Spectroscopic parameters of single-stranded FIT–PNA **4** before and after addition of matched and single-mismatched DNA **2**.

| PNA | | $\lambda_{max(abs)}$ [nm][a] | | $\varepsilon_{max(abs)}$ [$M^{-1}cm^{-1}$][b] | | $\lambda_{max(em)}$ [nm][c] | | $\phi_{em}$[d] | | $F_{ds}/F_{ss}$[e] | |
|---|---|---|---|---|---|---|---|---|---|---|---|
| | | single strand | double strand | single strand | double strand | single strand | double strand | single strand | double strand | matched | mismatched |
| **4**aa | a-TO-a | 516 | 514 | 38000 | 51000 | 543 | 531 | 0.03 | 0.27 | 28.2 | 13.0 |
| **4**tt | t-TO-t | 515 | 516 | 16000 | 25000 | 533 | 531 | 0.03 | 0.20 | 16.6 | 3.4 |
| **4**gg | g-TO-g | 517 | 518 | 57000 | 73000 | 540 | 536 | 0.04 | 0.16 | 4.8 | 9.8 |
| **4**cc | c-TO-c | 517 | 518 | 35000 | 43000 | 537 | 536 | 0.03 | 0.13 | 4.2 | 3.0 |
| **4**at | a-TO-t | 517 | 514 | 19000 | 23000 | 536 | 530 | 0.03 | 0.23 | 14.0 | 4.5 |
| **4**ag | a-TO-g | 513 | 515 | 59000 | 90000 | 548 | 535 | 0.05 | 0.25 | 18.0 | 24.0 |
| **4**ac | a-TO-c | 519 | 516 | 58000 | 80000 | 539 | 534 | 0.03 | 0.21 | 22.8 | 12.8 |
| **4**gc | g-TO-c | 517 | 518 | 58000 | 71000 | 536 | 537 | 0.02 | 0.14 | 6.8 | 3.9 |

[a] Wavelength of absorbance maximum. [b] Extinction coefficient at wavelength of absorbance maximum. [c] Wavelength of fluorescence-emission maximum. [d] Fluorescence quantum yield. [e] Ratio between fluorescence intensities at 525 nm after ($F_{ds}$) and before ($F_{ss}$) addition of DNA.

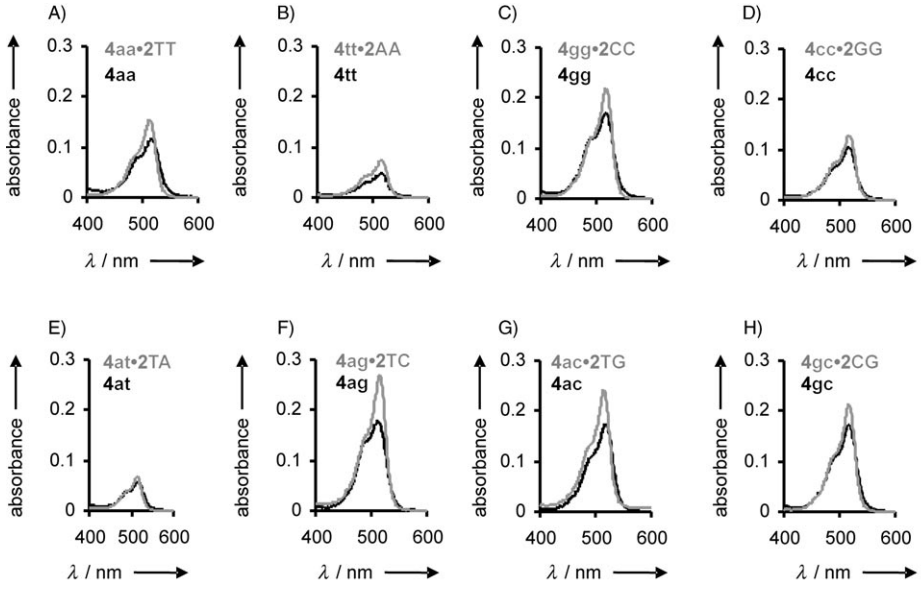


Figure 4. Absorbance spectra of FIT–PNA before (black) and after (gray) addition of an equimolar amount of complementary DNA: A) a-TO-a (**4**aa, **4**aa•**2**TT); B) t-TO-t (**4**tt, **4**tt•**2**AA); C) g-TO-g (**4**gg, **4**gg•**2**CC); D) c-TO-c (**4**cc, **4**cc•**2**GG); E) a-TO-t (**4**at, **4**at•**2**TA); F) a-TO-g (**4**ag, **4**ag•**2**TC); G) a-TO-c (**4**ac, **4**ac•**2**TG); and H) g-TO-c (**4**gc, **4**gc•**2**CG). Measurement conditions: 3 μM FIT–PNA and 3 μM DNA (added after measurement of single-strand PNA) in degassed buffer (NaCl (100 mM), $NaH_2PO_4$ (10 mM) at pH 7.0).

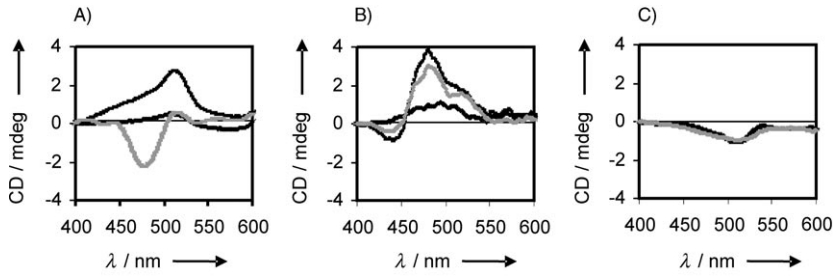


Figure 5. Induced CD spectra of TO–PRO1 in A) DNA•DNA duplex **1**•**2** and B) PNA•DNA duplex **3**•**2** at mixing ratios (dye/bp) 1:10 (gray curve), 1:4 (upper black curve), and 1:2.5 (lower black curve). C) CD spectra of FIT–PNA•DNA duplex **5**t•**6**TA (black curve) and FIT–PNA•DNA duplex **4**gc•**2**CG (gray curve). Spectra were set to zero at 400 nm. Measurement conditions: 52 μM duplex **1**•**2** or **3**•**2** and various amounts of dye, or 3 μM FIT–PNA **5**t or **4**gc, and DNA **6**TA or **2**CG in buffer (NaCl (100 mM), $NaH_2PO_4$ (10 mM) at pH 7.0) at 15 °C.

High fluorescence quantum yield ($\phi_{em}=0.27$) was obtained for duplex **4**aa•**2**TT, which featured two adenines as intra-strand stacking partners. The high $\phi_{em}$ values of 0.21 and 0.25 obtained for duplexes **4**ac•**2**TG (a-TO-c) and **4**ag•**2**TC (a-TO-g), respectively, and the comparatively low $\phi_{em}$ of 0.13, 0.14, and 0.16 in duplexes **4**cc•**2**GG (c-TO-c), **4**gc•**2**GC (g-TO-c), and **4**gg•**2**CC (g-TO-g), respectively, suggested that one guanine–cytosine pair was not sufficient to quench the TO fluorescence. The high fluorescence quantum yield ($\phi_{em}=0.23$) of thiazole orange forced to intercalate between an a–T and a t–A base pair in **4**at•**2**TA is remarkable as the noncovalent association of TO–PRO1 to the self-complementary $(dAdT)_{10}$ duplex has been reported to result in a lower quantum yield of 0.13.[9] TO–PRO1 showed higher fluorescence quantum yields ($\phi_{em}=0.23$) in self-complementary $(dGdC)_6$.[9] In contrast, forced intercalation between c and g in **4**cg•**2**GC gave a low $\phi_{em}$ of 0.14. These results suggest that TO fluorescence not only responds to the base composition of the near environment, but also to the TO–nucleic acid binding mode, and perhaps also to more subtle changes, such as local conformations. The latter feature is considered important for applications in single-base-mutation analysis (see below).

The responsiveness of TO to changes in the environment was most noticeable in measurements of fluorescence intensity, which is the monitored pa-

  

Table 3. Melting temperatures of FIT–PNA·DNA duplexes.

| | | $T_M$ [°C][a] |
|---|---|---|
| **5**t | gccgt-a-TO-t-agccg | 68 |
| **6**TA | CGGCA-T- T-A-TCGGC | – |
| **5**t | gccgt-a-TO-t-agccg | 71 |
| **6**HA | CGGCA-T- H-A-TCGGC | – |
| **5**h | gccgt-a-TO-h-agccg | 59 |
| **6**TA | CGGCA-T- T-A-TCGGC | – |

[a] Determined as the maximum of the negative first derivative of the denaturation curves measured at 260 nm. (h = abasic site PNA monomer shown in Figure 1, H = tetrahydrofuran nucleotide shown in Figure 1. Measurement conditions: 1 μM duplex, NaCl (100 mM), $NaH_2PO_4$ (10 mM), pH 7.0, 20–85 °C, 1 °C min$^{-1}$ heating rate.

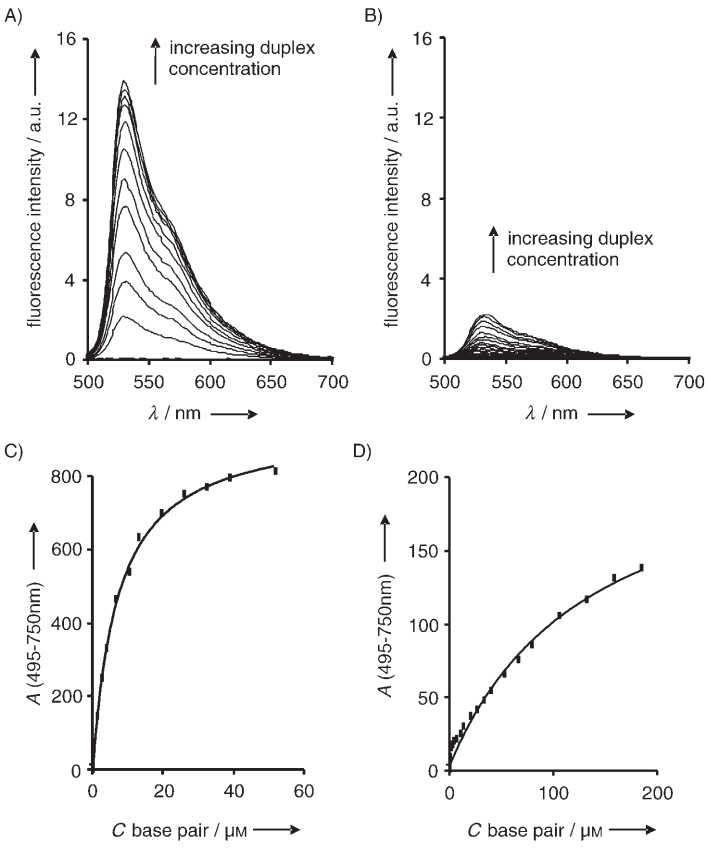


Figure 6. Fluorescence emission of TO–PRO1 before and after addition of A) DNA·DNA duplex **1·2** (0.1, 0.2, 0.3, 0.5, 0.7, 1.0, 1.5, 2.0, 2.5, 3.0, and 4.0 μM) and B) PNA·DNA duplex **3·2** (0.1, 0.2, 0.3, 0.5, 0.7, 1.0, 1.5, 2.0, 2.5, 3.0, 4.0, 5.0, 6.0, 8.0, 10.0, 12.0, and 14.0 μM). C) and D) Fluorescence titration data and binding curves obtained by curve fitting of integrated fluorescence-emission (495–750 nm) versus concentration of base pairs. Measurement conditions: see legend of Figure 2. ($A$ = integrated emission between 495 and 750 nm.)

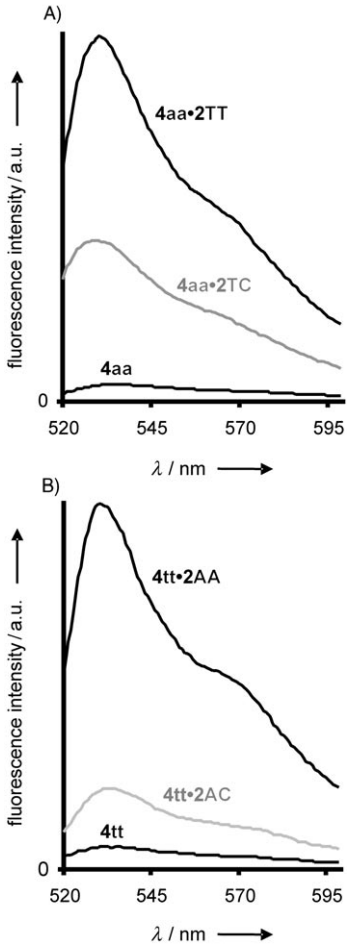


Figure 7. Fluorescence-emission spectra of FIT–PNA before (lower black curve) and after addition of an equimolar amount of complementary DNA (upper black curve) or mismatched DNA (gray curve): A) a-TO-a (**4**aa, **4**aa·**2**TT, **4**aa·**2**TC); B) t-TO-t (**4**tt, **4**tt·**2**AA, **4**tt·**2**AC). Measurement conditions: 1 μM FIT–PNA and 1 μM DNA (added after measurement of single-strand PNA) in degassed buffer (NaCl (100 mM), $NaH_2PO_4$ (10 mM) at pH 7.0).

rameter in applications. Table 2 also lists fluorescence enhancements $F_{ds}/F_{ss}$ (ds = double stranded, ss = single stranded) upon hybridization to perfectly matched target DNA and single-mismatched DNA. It became apparent that the fluorescence of conjugated thiazole orange increased in intensity upon hybridization in any studied sequence. Highest fluorescence increases (12 to 28-fold) were obtained upon formation of duplexes in which TO was allowed to stack to at least one adenine–thymine base pair. Interestingly, in six of the eight tested probes the presence of a single-base mismatch resulted in attenuated intensities of TO fluorescence emission, showing only 25–80% of the fluorescence increases observed for matched hybridization. For example, the fluorescence intensity of single strands **4**aa and **4**tt was enhanced by factors of 28 and 17, respectively, upon matched hybridization, whereas only 13- and 3-fold fluorescence increases were obtained upon single-mismatched hybridization, respectively (Figure 7). This property is of interest in DNA mutation analysis as it provides an additional level of sequence discrimination other than by hybridization alone. The two probes **4**gg and **4**ag, in which single-mismatched duplexes fluoresced with higher intensity than matched duplexes, featured g–G mismatched base pairs as opposed to g–C matched base pairs. These results support the notion that

  

Table 4. Fluorescence-decay analysis of TO–PRO1 and FIT–PNA.

| | | | $\tau_{ns}$ $(a)$[a] | | | | $\chi^2$ |
|---|---|---|---|---|---|---|---|
| | | | very fast | fast | medium | slow | |
| TO–PRO1 | | +polymer | | | 1.38 (14.0) | 3.60 (86.0) | 1.00[c] [2.13][b] |
| | | +**1**·**2** | | 0.33 (28.6) | 1.36 (39.3) | 2.74 (32.1) | 1.09[d] [1.71][c] |
| | | +**3**·**2** | 0.04 (28.6) | 0.35 (34.8) | 1.37 (27.8) | 3.47 (8.8) | 1.06[e] [1.29][d] |
| **4**aa (a-TO-a) | ss | **4**aa | 0.05 (50.2) | 0.48 (41.0) | 1.49 (6.7) | 3.64 (2.2) | 1.11[e] [1.54][d] |
| | dsmt[f] | **4**aa·**2**TT | | 0.39 (22.3) | 1.39 (37.9) | 3.03 (39.8) | 1.05[d] [1.51][c] |
| | dsmm[g] | **4**aa·**2**TC | | 0.28 (52.9) | 1.10 (34.7) | 3.31 (12.3) | 1.05[d] [2.37][c] |
| **4**at (a-TO-t) | ss | 4at | 0.05 (32.4) | 0.26 (39.5) | 1.24 (19.0) | 3.95 (9.1) | 1.08[e] [1.24][d] |
| | dsmt | **4**at·**2**TA | | 0.35 (26.6) | 1.54 (35.1) | 3.57 (38.3) | 1.04[d] [1.68][c] |
| | dsmm | **4**at·**2**TC | | 0.32 (43.7) | 1.29 (38.4) | 3.55 (17.8) | 1.04[d] [2.67][c] |
| **4**ag (a-TO-g) | ss | **4**ag | 0.07 (41.2) | 0.38 (32.2) | 1.28 (21.2) | 3.17 (5.4) | 1.08[e] [1.55][d] |
| | dsmt | **4**ag·**2**TC | | 0.34 (17.0) | 1.22 (46.5) | 2.63 (36.5) | 1.05[d] [1.31][c] |
| | dsmm | **4**ag·**2**TG | | 0.33 (29.0) | 1.50 (40.4) | 3.44 (30.6) | 1.02[d] [1.95][c] |
| **4**ac (a-TO-c) | ss | **4**ac | 0.04 (42.9) | 0.32 (22.1) | 1.05 (31.9) | 2.67 (3.1) | 1.03[e] [1.45][d] |
| | dsmt | **4**ac·**2**TG | | 0.32 (19.8) | 1.28 (51.5) | 2.55 (28.7) | 1.00[d] [1.44][c] |
| | dsmm | **4**ac·**2**TC | | 0.22 (52.5) | 1.06 (36.1) | 2.88 (11.5) | 1.11[d] [4.46][c] |
| **4**gc (g-TO-c) | ss | **4**gc | 0.04 (33.2) | 0.24 (45.3) | 1.10 (15.5) | 3.38 (5.7) | 1.02[e] [1.33][d] |
| | dsmt | **4**gc·**2**CG | | 0.37 (26.0) | 1.26 (53.5) | 2.33 (20.5) | 1.07[d] [1.74][c] |
| | dsmm | **4**gc·**2**CC | | 0.27 (55.8) | 1.11 (25.2) | 2.66 (19.0) | 1.07[d] [3.28][c] |

[a] $\tau_{ns}$ = fluorescence-decay lifetime [ns]; relative amplitudes $a$ in the emission-decay fits are given as decimal fractions in parentheses. [b, c, d, e] $\chi^2$ obtained by monoexponential, biexponential, triexponential, and tetraexponential, respectively, fitting of fluorescence-decay curves. Values are $\chi^2$ for optimal $n$-exponential fitting, values in brackets are $\chi^2$ for $(n-1)$-exponential fitting. [f] dsmt = double-stranded match. [g] dsmm = double-stranded mismatch.

TO responds to local changes in the π-stacking environment, and it is conceivable that the congested π stack provided by a g–G mismatch in **4**gg and **4**ag closed nonradiative-decay channels more efficiently than a c–G match.

**Time-resolved fluorescence**: To examine more closely the fluorescent species, fluorescence lifetimes were measured by time-correlated single-photon counting (TCSPC). Firstly, TO–PRO1 was immobilized in a polyvinyl alcohol film to explore its properties in a highly viscous medium. A biexponential fit with decay times of 3.6 and 1.38 ns adequately described the fluorescence-decay curve, as demonstrated by a low $\chi^2$ of 1.0 obtained for the biexponential fit (Table 4). Three different decay times were observed for FIT–PNA containing duplexes and for TO–PRO1 bound to DNA·DNA duplex **1**·**2** (Figure 8). In contrast, a tetraexponential was necessary to fit the fluorescence decay of single-stranded FIT–PNA and of TO–PRO1 complexed to PNA·DNA duplex **3**·**2**. Attempts to describe the decay curves with a triexponential resulted in unacceptably high $\chi^2$ of 1.29. The decay processes can be classified into very fast decay processes (within 0.04–0.07 ns), fast decays (within 0.22–0.48 ns), and medium and slow decays (within 1.05–1.54 and 2.33–3.95 ns, respectively). As can be seen from Table 4, the two short decay times of single-stranded FIT–PNA have high amplitudes (65–91 %). Remarkably, addition of complementary DNA to FIT probes led to the complete disappearance of the very fast decay process. The very fast decay process was also absent in TO–PRO1 complexed to DNA·DNA duplex **1**·**2**. In contrast, the very fast decay still occurred in complexes of TO–PRO1 and PNA·DNA duplex **3**·**2**. A likely assignment to this decay process is contact of unconstrained TO with water and it seems that enforced intercalation in PNA–DNA effectively protected the TO dye from water, whereas association of free TO–PRO1 with PNA·DNA provided, amongst others, water-exposed fluorescent species.

The formation of matched FIT–PNA duplexes decreased the population of fast-decaying species and increased the population of TO fluorophores emitting with the two longer decay times. The hybridization-induced change in the decay times was less clear because both increases and decreases in short and medium decay times were observed. However, a decrease in the long decay time was found in all cases of matched hybridization studied. Interestingly, the duration of the medium and slow decay processes showed a correlation with the absorbance. For example, these two decay times were shortest in duplexes containing FIT–PNA **4**ag (1.22 and 2.63 ns, $\varepsilon_{max}$ = 89 800), **4**gg (1.28 and 2.55 ns, $\varepsilon_{max}$ = 80 100), and **4**gc (1.26 and 2.33 ns, $\varepsilon_{max}$ = 70 900 $M^{-1}cm^{-1}$), which had significantly higher absorbances than complexes **4**tt (1.39 and 3.03 ns, $\varepsilon_{max}$ = 24 600) and **6** (1.54 and 3.57 ns, $\varepsilon_{max}$ = 22 600 $M^{-1}cm^{-1}$). The transition of FIT single strands to single-mismatched duplexes showed noteworthy behavior. Although the amplitude of the two slow decay processes still increased with single-mismatched hybridization (albeit not to the extent observed in matched hybridization), the fast decay process showed increases in amplitudes rather than the decreases found in matched hybridization. For example, the population of the fluorescing species in single-stranded FIT–PNA **4**aa that decayed with a short decay time changed from 41 to 53 % upon formation of the mismatched complex **4**aa·**2**TC. This population increase of fast decay species was even more dramatic (22 to 53 %) with FIT–PNA **4**ac. Furthermore, the short decay times of TO in single-mismatched duplexes were shorter (by 0.01–0.11 ns) than in matched duplexes, and it can be concluded that the presence of mismatched base pairs apparently facilitated the

  

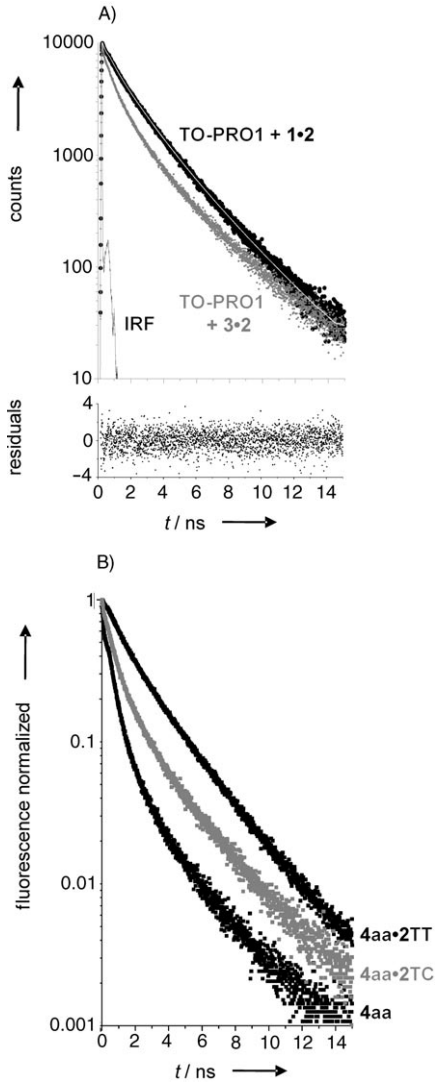


Figure 8. A) Fluorescence-decay curves of TO–PRO1 after addition of DNA•DNA duplex **1•2** (black curve) and PNA•DNA duplex **3•2** (gray curve). Lower part: residuals of the fit of the black decay curve. B) Normalized fluorescence-decay profiles of FIT–PNA **4**aa (a-TO-a) in single-stranded form (lower black curve) and after mismatched (gray curve) and matched (upper black curve) hybridization. For lifetimes and amplitudes, see Table 4. (Conditions: $\lambda_{ex} = 532$ nm, $\lambda_{det} = 580$ nm.)

fast decay process, which often occurred even more rapidly than in the single-stranded form.

Comparison of the two slower decay processes in mismatched duplexes with the corresponding processes in matched duplexes revealed a complex interplay between increases and decreases in decay times and amplitude factors. For example, the FIT–PNA **4**ag containing TO between adenine and guanine featured higher fluorescence increases upon mismatched hybridization than upon matched hybridization, which was reflected by a marked increase in the medium decay time (by 0.22 ns) and an exceptional prolongation (by 0.27 ns versus a decrease by 0.54 ns in the case of matched hybridization) of the long decay time. In all other studied mismatched duplexes the medium decay process occurred faster than (by 0.15–0.29 ns), but with similar amplitude to, that in matched duplexes. In contrast, the longer decay times were similar or longer (by 0.28–0.33 ns) in the presence of single mismatches, albeit at the cost of amplitude. As a result, the averaged fluorescence lifetime of the TO excited state is reduced by 0.31–0.88 ns in the presence of single-base mismatches in **4**aa, **4**at, **4**ac, and **4**gc (data not shown).

## Discussion

**TO–PRO1**: The binding of TO and TO–PRO1 to double-stranded DNA involves several binding modes, the most important being intercalation and minor-groove binding.[2,9–11] The resulting increases in TO fluorescence emission are key to various DNA detection assays. The data presented show that TO–PRO1 also binds to PNA•DNA duplexes, as evidenced by decreases in TO absorbance and increases in fluorescence emission. This could provide new opportunities for the detection of probe–target complexes in PNA-based hybridization assays. However, data from fluorescence titrations showed that complexes of TO–PRO1 and PNA•DNA duplex **3•2** are less stable than complexes with DNA•DNA duplex **1•2** ($K_{app} = 7.3$ and 134 μM per base pair, respectively). Previous investigations by Nordén showed that traditional intercalators, such as ethidium, methoxypsoralen, and ruthenium dipyridinophenazine complexes, failed to bind to PNA•DNA duplexes, whereas minor groove binders, such as DAPI (4′,6-diamidino-2-phenylindole) and distamycin, showed modest binding affinities.[41] Armitage demonstrated that the minor groove of PNA•DNA duplexes provides a high-affinity template for the aggregation of the symmetrical cyanine dye $DiSC_2$.[42,43] We have not attempted to resolve the stoichiometry of TO–PRO1•PNA•DNA complexes. However, we note that in PNA•DNA the CD couplet, indicative for dye–dye interactions, appears at lower dye concentrations than in DNA•DNA complexes. Dye–dye interactions can only occur at nonintercalative binding sites at the duplex exterior. Hence, it is reasonable to assume that TO–PRO1 more readily accommodates the extrahelical binding sites of PNA•DNA, presumably due to a lack of high-affinity intrahelical binding sites (intercalation). This interpretation is in line with results from fluorescence-decay analysis, which revealed that TO–PRO1 in the complex with the PNA•DNA duplex **3•2** featured a very short decay time (0.04 ns) attributed to contact with water.

**TO–PNA (FIT–PNA)**: The increased nearest-neighbor dependence of TO absorbance in single-stranded and double-stranded FIT–PNA ($\varepsilon_{max} = 16000$–$59000$ and 23000–$90000\,M^{-1}cm^{-1}$, respectively) is remarkable. At present we do not have an explanation for this, but it may be reasonable to presume ground-state interactions between TO and nucleobases, which may be induced/facilitated by the use of TO as a surrogate base. The increases in steady-state fluorescence, the disappearance of the very short fluorescence-

  

decay process, and the increased amplitude of long decay processes indicate that double-strand formation results in an efficient protection from water and a rigidification of the TO environment. The marked nearest-neighbor dependence of TO absorbance and the negative band in the induced circular dichroism spectrum that coincides with the TO absorbance spectrum are most readily explained if an intrahelical conformation of TO in FIT–PNA·DNA duplexes is assumed. The opposing base may accommodate an extrahelical conformation or may intercalate above or below TO. In any case, it is difficult to imagine that both the polycyclic TO and the opposing nucleobase can simultaneously intercalate without detriment to duplex stability. Indeed, the higher $T_M$ of duplexes in which TO is lacking an opposite base (**5**t·**6**HA, Table 3) are in agreement with an intrahelical position of TO. In contrast, TO–PRO1 seems to occupy extrahelical binding sites of PNA·DNA duplexes, such as **3·2** (see above). The opposite binding modes nicely illustrate how a chromophore can be forced to intercalate at a specific position, despite having alternative binding preferences.

Given the precisely located intrahelical position of TO in nucleic acid duplexes, it is possible to explore the influence of individual adjacent nucleobases on TO photophysical properties. The fluorescence quantum yields were highest in duplexes that contained adenine–thymine base pairs as the TO stacking partner and lowest with adjacent guanine–cytosine base pairs. This data is in contrast to results of previous observations in which TO and TO–PRO1 showed higher fluorescence quantum yields in GC-rich rather than AT-rich duplexes.[9,10] These previous observations suggested that TO would be excluded from excited-state electron-transfer quenching by guanine, even though estimations of the free energy revealed that this process may occur spontaneously.[9] In measurements of noncovalently associated dyes the identity of the fluorescence species (intercalated, minor-groove-bound, backbone-associated) is less-clearly defined than in FIT–PNA. Hence, it is conceivable that in previous investigations TO also occupied binding sites in which the electronic coupling to adjacent nucleobases was hampered. In contrast, TO in FIT–PNA showed strong interactions with adjacent nucleobases that are demonstrated best by the pronounced nearest-neighbor dependence of the absorbance spectra. Based on our data we can not exclude the possibility of electron transfer from guanine to the excited state of the intercalated TO. We speculate that forced intercalation stabilizes intercalative TO interaction modes not favored in noncovalent aggregates. However, one guanine is not sufficient to quench the fluorescence of the FIT–PNA duplex, as indicated by high fluorescence quantum yields of complexes that featured at least one AT pair as stacking partner. This is an encouraging result as far as a general applicability in DNA detection assays is concerned. However, if the presence of one GC pair requires to be sensed, time-resolved fluorescence is a suitable means (see below).

**Time-resolved fluorescence**: The TO–nucleic acid complexes studied here displayed three or four decay times. The shortest decay time, which was assigned to a water-accessible fluorescent species, was detected only for single-stranded FIT–PNA and the relatively weak complexes of TO–PRO1 and PNA·DNA duplex **3·2**. Only three decay times were observed for FIT–PNA duplexes and for complexes of TO–PRO1 and DNA·DNA duplex **1·2**. The decay times are in agreement with those determined by Netzel and co-workers for complexes of TO–PRO1 and calf thymus DNA.[9] Melvin and co-workers studied DNA·DNA duplexes in which TO was appended through a flexible tether to the internucleotidic phosphate bridge.[26] They identified four decay times that are different from those reported by us and Netzel. The differences were explained by Melvin to arise from the use of different oligonucleotide sizes and sequences.

The experiments with polymer-immobilized TO–PRO1 suggest that the two slower decay processes found in nucleic acids are a characteristic of TO species in a highly viscous environment. These species presumably are in tight contact with a rigid scaffold that prevents twisting around the TO methine bridge. In FIT–PNA, the rigid scaffold is provided by the helical base stack. One could assume that the strong GC pairs confer a less-flexible stacking environment than AT pairs. In the absence of electronic coupling between TO and the adjacent nucleobases one may expect longer decay times and, thus, greater fluorescence increases for duplexes containing TO flanked by GC than by AT base pairs. However, the opposite was observed, as the presence of GC base pairs as stacking partner led to a reduction in the two longer decay times (Table 4, compare **4**aa and **4**at with **4**gc, **4**ac, and **4**ag). These observations indicate that the decay processes characteristic for rigidified TO are also those that showed the highest responsiveness to the identity of the adjacent nucleobases. Therefore, these processes may be suitable for exploring base-pair-specific binding modes.

The transition from single-stranded to double-stranded FIT–PNA was dominated by the disappearance of the very fast decay process. However, the slow decay process also showed high hybridization-induced responses (decrease in decay time by 0.12–1.03 ns and increase in amplitude by factors of 4–18). Although the fast decay process showed relatively little sensitivity to double-strand formation, it was this decay along with the slow decay process that exhibited the highest responsiveness to the presence of single-mismatched stacking partners. One of the five FIT–PNA complexes studied in time-resolved fluorescence measurements showed greater fluorescence in the mismatched duplex than in the matched duplex. In this case (FIT–PNA **4**ag), the slow decay process of TO in the mismatched duplex showed only a minor decrease in amplitude that was overcompensated by a large increase in the decay time relative to matched duplexes. Interestingly, the fast decay process still responded, as evidenced by a 1.6–2.6-fold increase in amplitude.

  

## Conclusion

We explored whether intercalated cyanine dyes, such as the thiazole orange dye used in nucleic acid staining, show optical properties that allow assignments of the DNA local environment. One requirement for this study was the ability to pinpoint the location of the affixed thiazole orange dye. The data collected from UV-visible absorbance, CD and fluorescence spectroscopy, and melting-curve analyses indicate that the use of thiazole orange as a surrogate base in FIT–PNA enabled the site-specific intercalation in PNA·DNA duplexes. In fact, intercalation was an enforced binding mode, as PNA·DNA duplexes appear not to provide high-affinity intercalation sites for TO–PRO1 and other established intercalators.

Notable hallmarks of TO steady-state optical properties in FIT–PNA·DNA duplexes are: 1) extraordinary dependence of the extinction coefficient ($\pm 60\%$ variation of the averaged $\varepsilon_{max}$ of $57\,000\,M^{-1}cm^{-1}$) on nearest-neighbor base pairs; 2) attenuated steady-state fluorescence emission if positioned between two GC base pairs and; 3) mostly low-emission quantum yields of TO adjacent to single-mismatched base pairs. Such effects are not observed in classical "noncovalent" TO—nucleic acid complexes. We assume that the close analogy of TO in FIT–PNA to canonical nucleobases enforces base-specific interaction modes that normally would be unable to compete with alternative, probably more-favored modes. These studies also highlighted four different fluorescence-decay processes that responded differently to changes in the TO environment: 1) a very fast fluorescence-decay process in the range of 0.04–0.07 ns that disappears upon double-strand formation; 2) a fast decay of between 0.22–0.48 ns that showed the highest sensitivity to local distortion of helix architecture and dynamics, such as those induced by mismatched base pairs; 3) a relatively unsusceptible medium decay process within 1.05–1.54 ns and; 4) a long decay of between 2.33–3.95 ns that is almost universally susceptible to changes conferred by hybridization and exchange of adjacent nucleobases. Therefore, the disappearance of the very fast decay process and the increase in the amplitude factor of the long decay process are reliable hybridization monitors that even may allow the discrimination of a GC environment from that of an AT. If, at the same time, an increase in the amplitude factor of the fast decay process is observed, it is likely that a distorted, mismatched duplex has formed.

We believe that the responsiveness of the optical properties to the stacking environment is a general feature of the forced intercalation mode and may, therefore, be applicable to other intercalator dyes, provided that short, nonflexible linkers are used. The sensitivity observed to changes in the nucleobase sequence should allow for the design of single-nucleotide-specific probes that omit the need for stringent hybridization conditions in DNA mutation analysis. However, it was noted that there may be mismatches, such as G–G mismatches, that still require stringency of hybridization or, alternatively, probes directed to the sense strand (or antisense strand). Exploration of FIT–PNA and other probes containing cyanine dyes of the thiazole orange family in DNA mutation analysis will be reported in due course.

## Experimental Section

Fluorescence spectroscopy was performed by using a Varian Cary Eclipse fluorescence spectrophotometer. A Varian Cary 100 Bio-UV/Vis spectrophotometer was used for optical and melting-curve analyses. CD measurements were performed by using a JASCO J-710 spectropolarimeter equipped with a Julabo F 25 as cooling device to control temperature. DNA was purchased from MWG-Biotech in HPSF quality. Water was purified by using a Milli-Q Ultrapure Water Purification System (Millipore). The stock solution of TO–PRO1 was prepared in methanol. The concentration was determined by using the molar extinction coefficient (in aqueous buffer) of $\varepsilon_{506} = 63\,000\,M^{-1}cm^{-1}$.

**Absorbance titration**: Solutions of duplexes of DNA·DNA **1·2** and PNA·DNA **3·2** were prepared by mixing equimolar amounts of corresponding oligonucleotides **1**, **2**, and **3** to a final duplex concentration of 70–80 μM. In titration experiments TO–PRO1 was added from the stock solution into a quartz fluorescence cuvette (4×10 mm) and diluted with aq. degassed buffer (NaCl (100 mM), $NaH_2PO_4$ (10 mM) at pH 7.0) to a final concentration of 0.5 μM. The absorbance spectrum was recorded at 25 °C. Duplexes from stock solutions were added as required to obtain the specified duplex concentration. To secure homogeneous binding of dye to duplexes, after each addition the solution was heated at 85 °C for 10 min and was then cooled to RT (5 °C min$^{-1}$). After 20 min the spectra were recorded at 25 °C. The spectra were corrected for dilution.

**Absorbance measurements**: Stock solutions of FIT–PNA (140–250 μM in $H_2O$) and DNA (140–250 μM in $H_2O$) were prepared. FIT–PNA solution was added into a quartz fluorescence cuvette (4×10 mm) and then diluted with aq degassed buffer (NaCl (100 mM), $NaH_2PO_4$ (10 mM) at pH 7.0) to a final concentration of 1 μM. The absorbance spectrum was recorded at 25 °C. DNA-target solution (3 nmol) was added to give a total volume of 1 mL and the absorbance spectrum was recorded after 20 min. The spectra were corrected for dilution.

**CD measurements**

*TO–PRO1 with **1·2** and **3·2** duplexes*: Solutions (52 μM) of DNA·DNA duplexes **1·2** and PNA·DNA duplexes **3·2** in degassed buffer (NaCl (100 mM), $NaH_2PO_4$ (10 mM) at pH 7.0) were prepared. Various amounts of TO–PRO1 were added from the stock solution. The solutions were heated at 85 °C for 10 min and then cooled to RT (5 °C min$^{-1}$). After 20 min the spectra were recorded at 15 °C.

*FIT–PNA*: FIT–PNA was added into a quartz cuvette (4×10 mm) and diluted with aq degassed buffer to a final duplex concentration of 3 μM. An equimolar amount of DNA target was added to give a total volume of 1 mL. CD spectra were recorded after 20 min at 15 °C.

**Melting-curve analysis**: UV melting curves were measured at 260 nm. A degassed aqueous solution of NaCl (100 mM) with $NaH_2PO_4$ (10 mM) at pH 7.0 was used as buffer. The DNA and PNA oligomers were mixed to 1:1 stoichiometry and the solutions were adjusted to a final duplex concentration of 1 μM. Prior to analysis, the samples were heated to 85 °C and then cooled within 1 h to the starting temperature of 20 °C. The samples were heated to 85 °C at a rate of 1 °C min$^{-1}$. $T_M$ values were defined as the maximum of the first derivative of the melting curve.

**Fluorescence titration**: Fluorescence titration experiments were performed with samples prepared for absorbance titration. Fluorescence spectra were recorded at 25 °C with excitation at 485 nm (excitation slit width: 5 nm; emission-slit width: 2.5 nm). Solvent background signals were subtracted.

**Fluorescence measurements**: Fluorescence measurements were performed with samples prepared for absorbance experiments. Fluorescence spectra were recorded at 25 °C with excitation at 485 nm (excitation-slit width: 5 nm; emission-slit width: 2.5 nm). Solvent background signals were subtracted.

  

**Quantum yield**: Quantum yields were determined relative to fluorescein in 0.1 N sodium hydroxide as described.[44] Fluorescence spectra were recorded at 25 °C with excitation at 485 nm. Emission was integrated between 495 and 750 nm. Solvent background signals were subtracted.

**Fluorescence decay**: Fluorescence lifetimes were measured by using the time-correlated single-photon counting (TCSPC) technique with the frequency-doubled pulses of a Ti:sapphire laser (Coherent Mira 900, 405 nm, FWHM 200 fs) for excitation. The instrument response function was 60 ps, as measured at the excitation wavelength with Ludox. The setup was previously described.[45] The excitation wavelength was 532 nm. Samples were measured in magic-angle configuration. Time-dependent fluorescence was monitored at different wavelengths in a range of 545–645 nm. A self-made routine was applied to minimize the least-squares error between the model function convoluted with the instrument response function (IRF) and the measured data set.

## Acknowledgements

O.S. acknowledges support from Schering AG.

[1] L. J. Kricka, *Ann. Clin. Biochemistry* **2002**, *39*, 114.
[2] L. G. Lee, C. H. Chen, L. A. Chiu, *Cytometry* **1986**, *7*, 508.
[3] H. S. Rye, S. Yue, D. E. Wemmer, M. A. Quesada, R. P. Haugland, R. A. Mathies, A. N. Glazer, *Nucleic Acids Res.* **1992**, *20*, 2803.
[4] C. Schneeberger, P. Speiser, F. Kury, R. Zeillinger, *PCR Methods Appl.* **1995**, *4*, 234.
[5] X. Jin, S. Yue, K. S. Wells, V. L. Singer, *FASEB J.* **1994**, *8*, 1266.
[6] S. J. Ahn, J. Costa, J. R. Emanuel, *Nucleic Acids Res.* **1996**, *24*, 2623.
[7] A. Larsson, C. Carlsson, M. Jonsson, N. Albinsson, *J. Am. Chem. Soc.* **1994**, *116*, 8459.
[8] C. Carlsson, A. Larsson, M. Jonsson, B. Albinsson, B. Nordén, *J. Phys. Chem.* **1994**, *98*, 10313.
[9] T. L. Netzel, K. Nafisi, M. Zhao, J. R. Lenhard, I. Johnson, *J. Phys. Chem.* **1995**, *99*, 17936.
[10] J. Nygren, N. Svanvik, M. Kubista, *Biopolymers* **1998**, *46*, 39.
[11] J. T. Petty, J. A. Bordelon, M. E. Robertson, *J. Phys. Chem. B* **2000**, *104*, 7221.
[12] J. Bunkenborg, N. I. Gadjev, T. Deligeorgiev, J. P. Jacobsen, *Bioconjugate Chem.* **2000**, *11*, 861.
[13] G. Cosa, K. S. Focsaneanu, J. R. N. McLean, J. P. McNamee, J. C. Scaiano, *Photochem. Photobiol.* **2001**, *73*, 585.
[14] C. Schweitzer, J. C. Scaiano, *Phys. Chem. Chem. Phys.* **2003**, *5*, 4911.
[15] V. Karunakaran, J. L. F. Lustres, L. J. Zhao, N. P. Ernsting, O. Seitz, *J. Am. Chem. Soc.* **2006**, *128*, 2954.
[16] H. P. Spielmann, D. E. Wemmer, J. P. Jacobsen, *Biochemistry* **1995**, *34*, 8542.
[17] J. P. Jacobsen, J. B. Pedersen, L. F. Hansen, D. E. Wemmer, *Nucleic Acids Res.* **1995**, *23*, 753.
[18] F. Johansen, J. P. Jacobsen, *J. Biomol. Struct. Dyn.* **1998**, *16*, 205.
[19] M. Petersen, A. A. Hamed, E. B. Pedersen, J. P. Jacobsen, *Bioconjugate Chem.* **1999**, *10*, 66.
[20] J. Bunkenborg, M. M. Stidsen, J. P. Jacobsen, *Bioconjugate Chem.* **1999**, *10*, 824.
[21] T. Ishiguro, J. Saitoh, H. Yawata, M. Otsuka, T. Inoue, Y. Sugiura, *Nucleic Acids Res.* **1996**, *24*, 4992.
[22] O. Seitz, F. Bergmann, D. Heindl, *Angew. Chem.* **1999**, *111*, 2340; *Angew. Chem. Int. Ed.* **1999**, *38*, 2203.
[23] N. Svanvik, A. Stahlberg, U. Sehlstedt, R. Sjoback, M. Kubista, *Anal. Biochem.* **2000**, *287*, 179.
[24] N. Svanvik, G. Westman, D. Y. Wang, M. Kubista, *Anal. Biochem.* **2000**, *281*, 26.
[25] N. Svanvik, J. Nygren, G. Westman, M. Kubista, *J. Am. Chem. Soc.* **2001**, *123*, 803.
[26] E. Privat, T. Melvin, U. Asseline, P. Vigny, *Photochem. Photobiol.* **2001**, *74*, 532.
[27] E. Privat, U. Asseline, *Bioconjugate Chem.* **2001**, *12*, 757.
[28] E. Privat, T. Melvin, F. Merola, G. Schweizer, S. Prodhomme, U. Asseline, P. Vigny, *Photochem. Photobiol.* **2002**, *75*, 201.
[29] X. F. Wang, U. J. Krull, *Anal. Chim. Acta* **2002**, *470*, 57.
[30] X. F. Wang, U. J. Krull, *Bioorg. Med. Chem. Lett.* **2005**, *15*, 1725.
[31] E. J. Fechter, B. Olenyuk, P. B. Dervan, *J. Am. Chem. Soc.* **2005**, *127*, 16685.
[32] R. Lartia, U. Asseline, *Chem. Eur. J.* **2006**, *12*, 2270.
[33] S. Prodhomme, J. P. Demaret, S. Vinogradov, U. Asseline, L. Morin-Allory, P. Vigny, *J. Photochem. Photobiol. B* **1999**, *53*, 60.
[34] R. Huber, N. Amann, H. A. Wagenknecht, *J. Org. Chem.* **2004**, *69*, 744.
[35] N. Amann, R. Huber, H. A. Wagenknecht, *Angew. Chem.* **2004**, *116*, 1881; *Angew. Chem. Int. Ed.* **2004**, *43*, 1845.
[36] K. Fukui, K. Tanaka, *Nucleic Acids Res.* **1996**, *24*, 3962.
[37] O. Köhler, D. V. Jarikote, O. Seitz, *ChemBioChem* **2005**, *6*, 69.
[38] O. Köhler, O. Seitz, *Chem. Commun.* **2003**, 2938.
[39] D. V. Jarikote, O. Köhler, E. Socher, O. Seitz, *Eur. J. Org. Chem.* **2005**, 3187.
[40] O. Köhler, D. V. Jarikote, O. Seitz, *Chem. Commun.* **2004**, 2674.
[41] P. Wittung, S. K. Kim, O. Buchardt, P. Nielsen, B. Nordén, *Nucleic Acids Res.* **1994**, *22*, 5371.
[42] J. O. Smith, D. A. Olson, B. A. Armitage, *J. Am. Chem. Soc.* **1999**, *121*, 2686.
[43] R. A. Garoff, E. A. Litzinger, R. E. Connor, I. Fishman, B. A. Armitage, *Langmuir* **2002**, *18*, 6330.
[44] J. N. Demas, G. A. Crosby, *J. Phys. Chem.* **1971**, *75*, 991.
[45] S. Makarov, C. Litwinski, E. A. Ermilov, O. Suvorova, B. Röder, D. Wöhrle, *Chem. Eur. J.* **2006**, *12*, 1468.
[46] V. Karunakaran, J. L. Pérez Lustres, L. Zhao, N. P. Ernsting, O. Seitz, *J. Am. Chem. Soc.* **2006**, *128*, 2954–2962.

Received: May 18, 2006
Published online: October 6, 2006

  